3D crack propagation analysis with PDS-FEM

M. L. L. Wijerathne (Lalith)
Hide Sakaguchi
Kenji Oguni
Muneo Hori

Japan Agency for Marine-Earth Science and Technology (JAMSTEC)
The University of Tokyo

Motivation

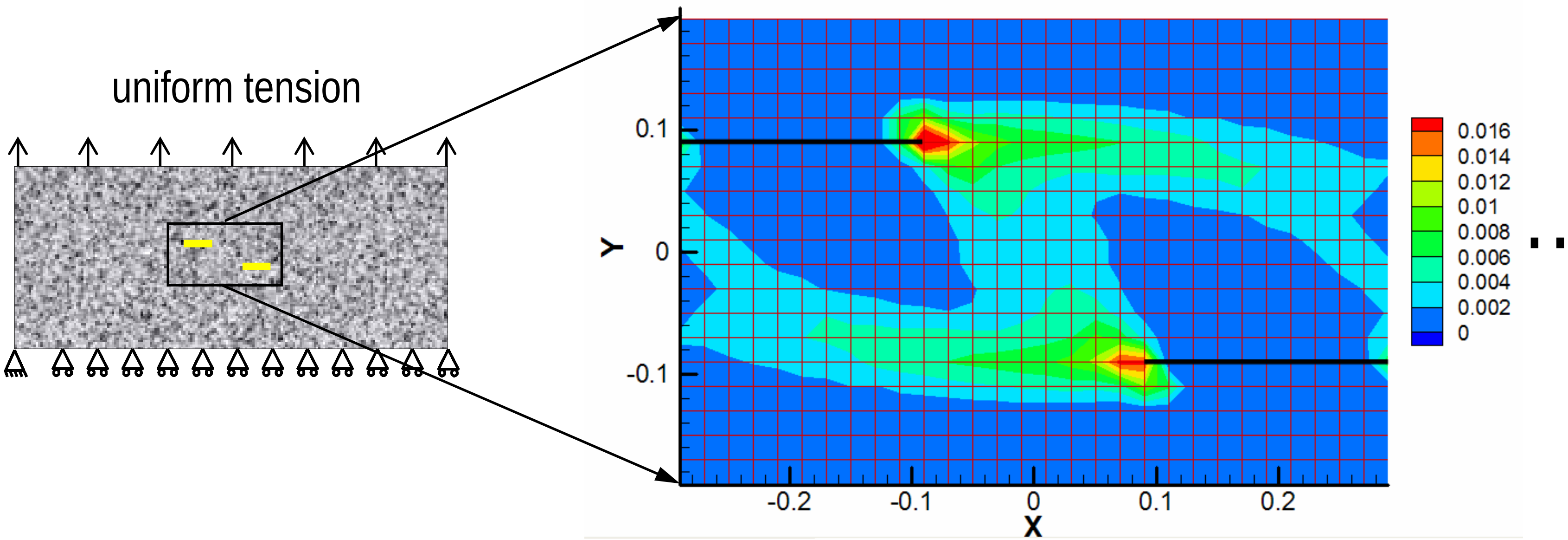

- Necessary to consider minor local heterogeneity
  - Size and distribution local heterogeneity cannot be measured
  - Monte-Carlo simulations with randomly distributed heterogeneity
- Meshless or adaptive methods are to complicated for stochastic studies
  - Difficult to introduce heterogeneity to the numerical model
  - Sophisticated and computationally intensive
- PDS-FEM provides simple means of modeling size and distribution of local heterogeneity with numerically efficient failure treatments

Organization

- Discretization scheme and formulation of PDS-FEM
- Failure treatment with torsional failure as an example
- Dynamic model and kidney stone breaking as an example

Background: two models of deformable body

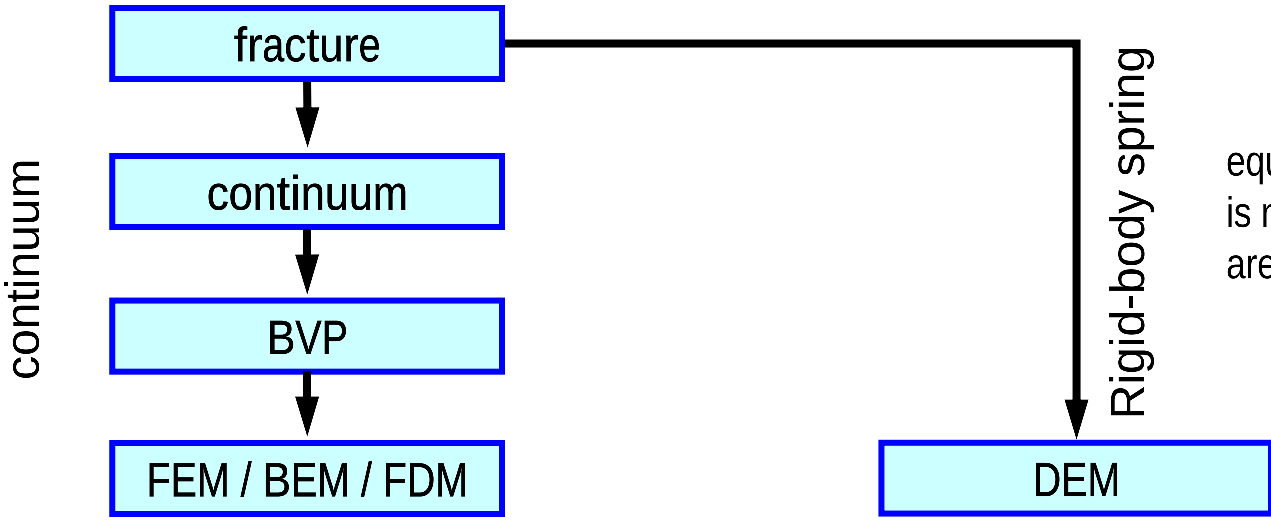

equivalence to continuum is not verified and springs are mysterious

difficult to deal with failure

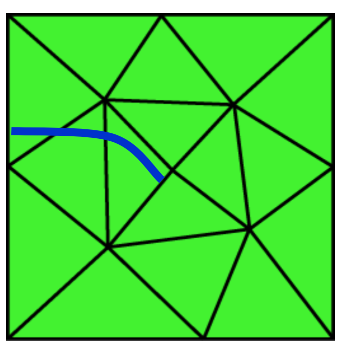

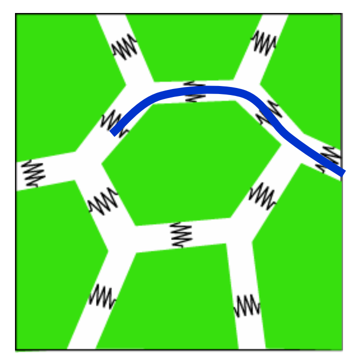

spring properties ?

Numerically intensive failure treatment

Efficient failure treatment

Discretization schemes of FEM and DEM

Ordinary FEM

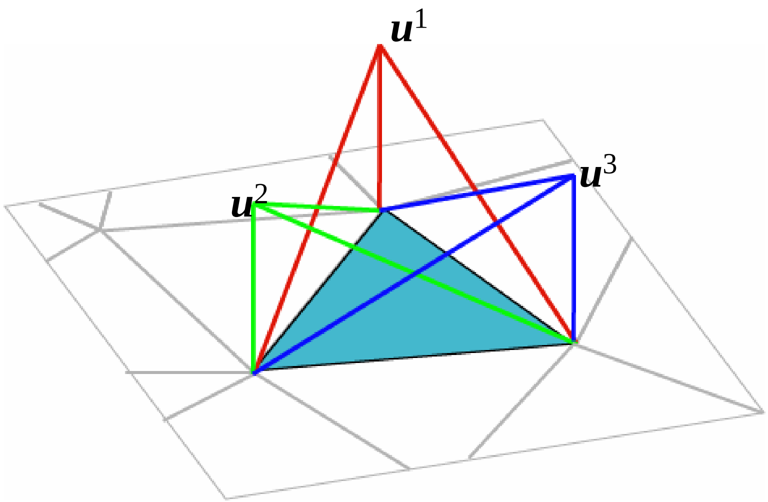

Smooth and overlapping shape functions

DEM

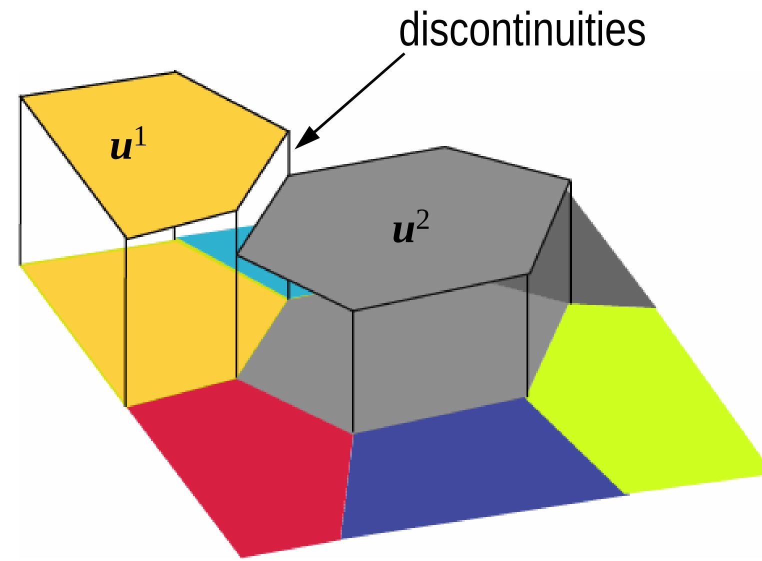

Particles can be interpreted as
non-overlapping shape functions

PDS-FEM: numerical method to solve BVP of a continuum with particle discretization

1-D particle discretization

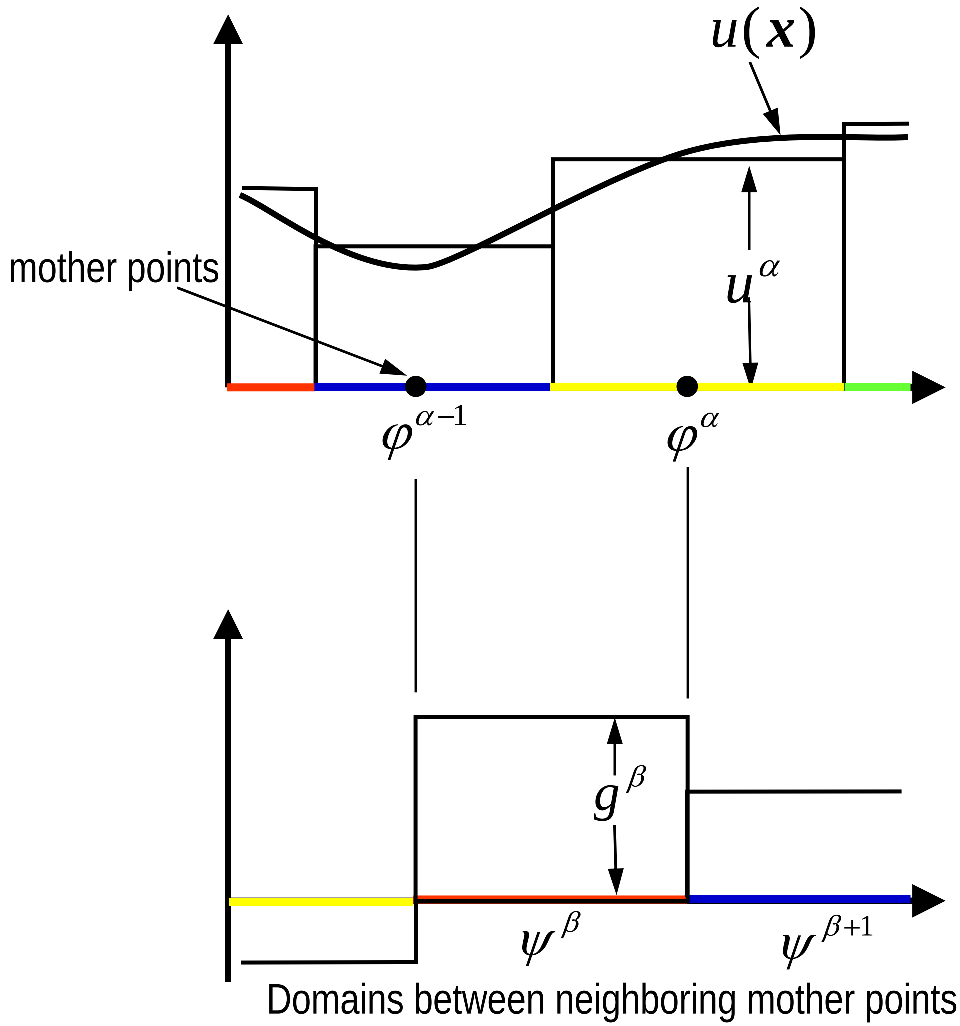

$$u^{d}(\boldsymbol{x}) = \sum_{\alpha} u^{\alpha} \varphi^{\alpha}(\boldsymbol{x})$$

f^{α} is the average value taken over the domain φ^{α}

$$\frac{df}{dx}(\boldsymbol{x}) = g(\boldsymbol{x}) = \sum_{\alpha} g^{\beta} \psi^{\beta}(\boldsymbol{x})$$

An average value for derivative is obtained on a conjugate geometry ψ^{α}

Function and derivative are discretized using conjugate geometries.

2D-Particle discretization

Voronoi tessellation for function $u(x)$

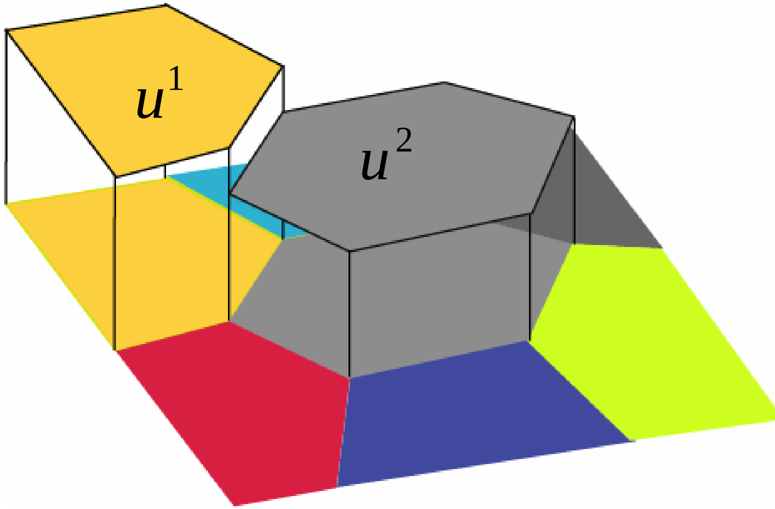

$$u^d(x) = \sum_{\alpha} u^{\alpha} \varphi^{\alpha}(x)$$

Delaunay tessellation for derivative $u_{,i}(\boldsymbol{x})$

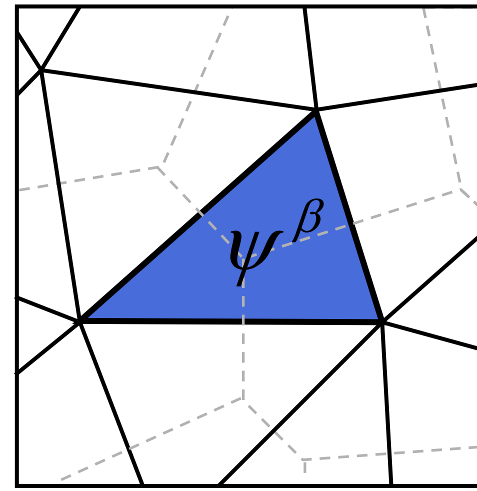

$$\frac{du^d(x)}{dx_j} = g_j^d(x) = \sum_{\beta} g_j^{\beta} \psi^{\beta}(x)$$

Function and derivative are discretized using conjugate geometries, Voronoi and Delaunay tessellations

Particle discretization for continuum: PDS-FEM

- Boundary Value Problem for Linear Elasticity

$$\begin{cases} (c_{ijkl}\, u_{k,l}(x)),_i + b(x)_j = 0 & \text{in } B \\ u(x)_i = \bar{u}_i & \text{on } \partial B \end{cases}$$

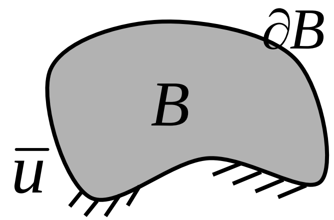

- Functional
  - Ordinary FEM functional $I(\mathbf{u}) = \frac{1}{2}\int_B u_{i,j} c_{ijkl} u_{k,l} - b_i u_i \, dv$
  - Functional used in PDS-FEM

$$J(u_j, \sigma_{ij}, \varepsilon_{ij}) = \int_B \tfrac{1}{2}\varepsilon_{ij} c_{ijkl} \varepsilon_{kl} - \sigma_{ij}(\varepsilon_{ij} - u_{j,i}) - b_j u_j \, dv$$

first variation

$$\delta J = -\int \delta u_j (\sigma_{ij,i} - b_j) + \delta\varepsilon_{ij}(\sigma_{ij} - c_{ijkl}\varepsilon_{kl}) + \delta\sigma_{ij}(\varepsilon_{ij} - u_{j,i}) \, dv$$

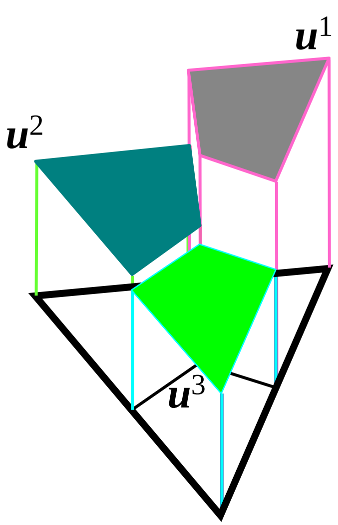

Particle discretization for continuum: PDS-FEM

1. Functional $J(u_j, \sigma_{ij}, \varepsilon_{ij}) = \int_B \frac{1}{2}\varepsilon_{ij} c_{ijkl} \varepsilon_{kl} - \sigma_{ij}(\varepsilon_{ij} - u_{j,i}) - b_j u_j \, dv$

2. Conjugate discretization

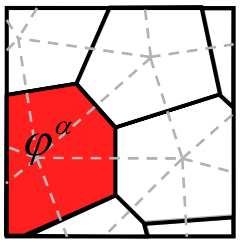

Voronoi

$$b_i(x) = \sum b_i^\alpha \varphi^\alpha(x)$$
$$u_i(x) = \sum u_i^\alpha \varphi^\alpha(x)$$

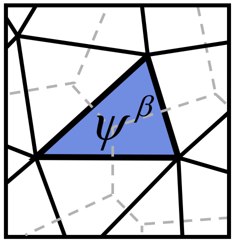

Delaunay

$$\sigma_{ij}(x) = \sum \sigma_{ij}^\beta \psi^\beta(x)$$
$$\varepsilon_{ij}(x) = \sum \varepsilon_{ij}^\beta \psi^\beta(x)$$
$$c_{ijkl}(x) = \sum c_{ijkl}^\beta \psi^\beta(x)$$

3. determination of u^α $\quad J = \frac{1}{2}\sum_{\alpha,\alpha'} K_{ik}^{\alpha\alpha'} u_i^\alpha u_k^{\alpha'} = \frac{1}{2}\sum_{\alpha,\alpha',\beta} \frac{\int_B \varphi,_j^\alpha \psi^\beta \, dv \; c_{ijkl}^\beta \int_B \varphi,_l^{\alpha'} \psi^\beta \, dv}{\int_B \psi^\beta \, dv} u_i^\alpha u_k^{\alpha'}$

4. With Voronoi and Delaunay tessellations, $K_{ik}^{\alpha\alpha'}$ coincides with stiffness matrix of FEM with linear characteristic functions

Organization

- Discretization scheme and formulation of PDS-FEM
- Failure treatment with torsional failure as an example
- Dynamic model and kidney stone breaking as an example

Failure treatment

stiffness matrix of FEM-β

$$\begin{bmatrix} [k_{11}] & \boxed{[k_{12}]} & [k_{13}] \\ [k_{21}] & [k_{22}] & [k_{23}] \\ [k_{31}] & [k_{32}] & [k_{33}] \end{bmatrix}$$

$$[k_{12}] = [k_{12}^{\text{direct}}] + [k_{12}^{\text{indirect}}]$$

Spring properties are rigorously determined with material properties; E and ν

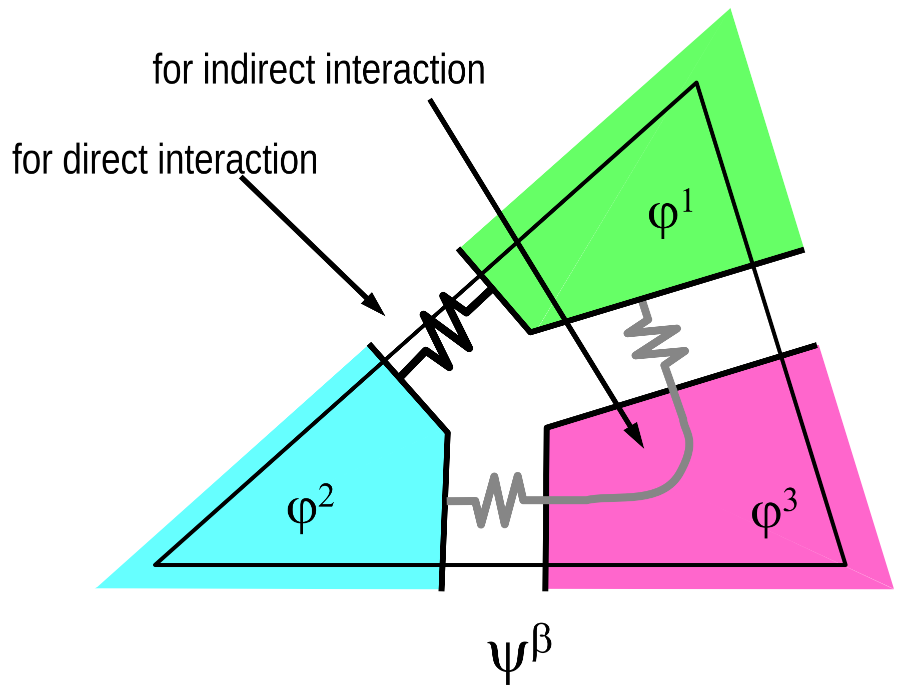

Failure is modeled by appropriately modifying the components of element stiffness matrix

Failure treatment: modeling brittle failure

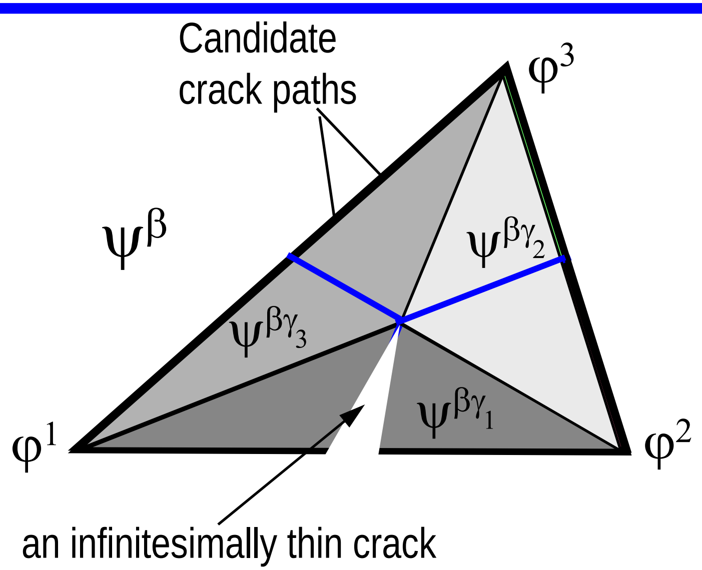

$$b_j^{\beta\alpha} = \frac{1}{\Psi^{\beta}} \int_B \varphi_{,j}^{\alpha} \psi^{\beta} \, dv$$

$$K_{ik}^{\alpha\alpha'} = \sum_{\beta} \left(b_j^{\beta\alpha} c_{ijkl}^{\beta} b_l^{\beta\alpha'} \right) \Psi^{\beta}$$

$$\mathbf{K} = \mathbf{B}^{\mathrm{T}} \mathbf{C} \mathbf{B}$$

$$d_j^{\beta\gamma\alpha} = \frac{1}{\Psi^{\beta}} \int_B \varphi_{,j}^{\alpha} \psi^{\beta\gamma} \, dv$$

$$\mathbf{B} = \left[\begin{array}{cc|cc|cc} b_1^{\beta\alpha_1} & & b_1^{\beta\alpha_2} & & b_1^{\beta\alpha_3} & \\ & b_2^{\beta\alpha_1} & & b_2^{\beta\alpha_2} & & b_2^{\beta\alpha_3} \\ b_2^{\beta\alpha_1} & b_1^{\beta\alpha_1} & b_2^{\beta\alpha_2} & b_1^{\beta\alpha_2} & b_2^{\beta\alpha_3} & b_1^{\beta\alpha_3} \end{array} \right] - \left[\begin{array}{cc|cc|cc} d_1^{\beta\gamma_1\alpha_1} & & d_1^{\beta\gamma_1\alpha_2} & & 0 & \\ & d_2^{\beta\gamma_1\alpha_1} & & d_2^{\beta\gamma_1\alpha_2} & & 0 \\ d_2^{\beta\gamma_1\alpha_1} & d_1^{\beta\gamma_1\alpha_1} & d_2^{\beta\gamma_1\alpha_2} & d_1^{\beta\gamma_1\alpha_2} & 0 & 0 \end{array} \right]$$

No new DOFs or elements are introduced to accommodate the new crack surface
Computational overhead is almost equal to re-computation of element stiffness matrix

Failure treatment of PDS-FEM is approximate

FEM

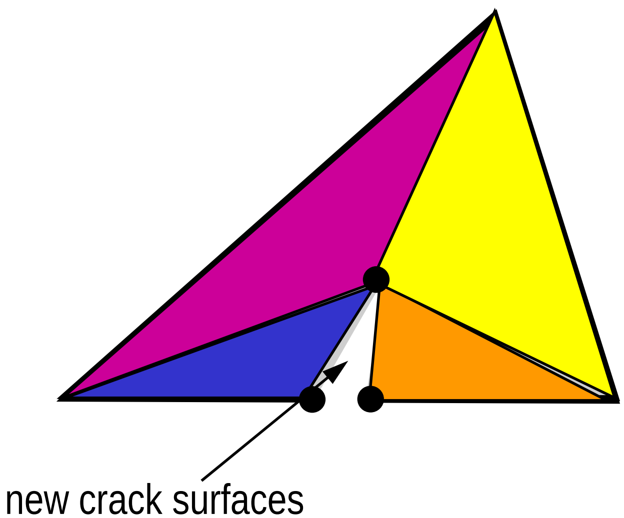

PDS-FEM

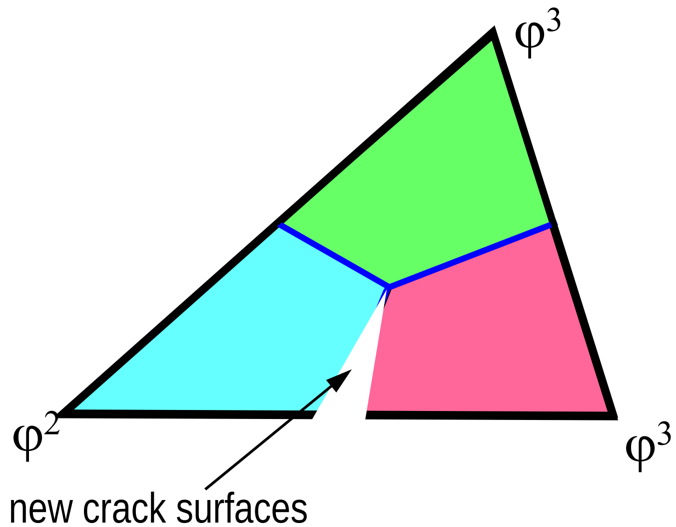

One new node ad four elements
are introduced

No new nodes are introduced

No new DOFs or elements are introduced to accommodate the new crack surface
Cannot guarantee the satisfaction of BCs on new crack surface

Accuracy of approximate failure treatment: problem setting

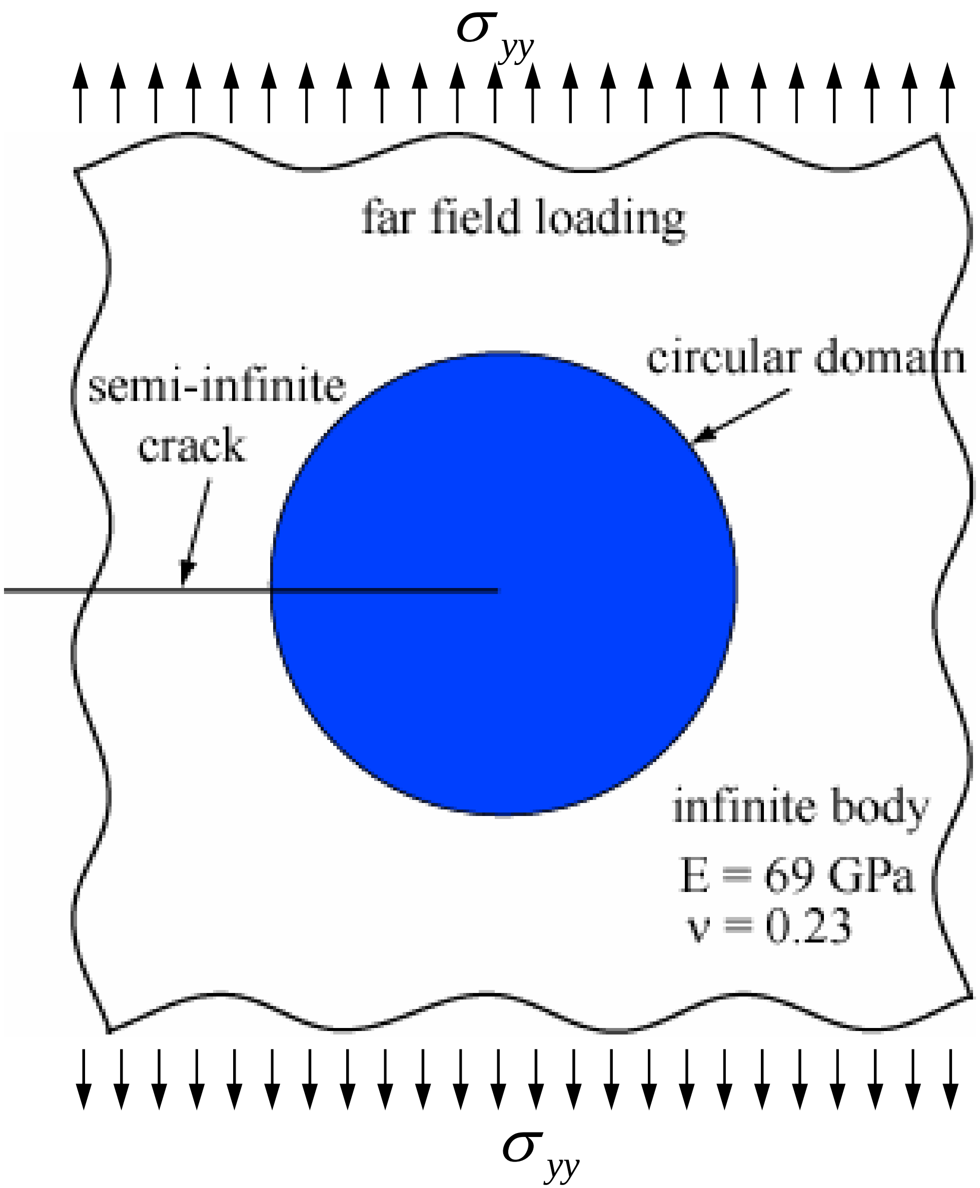

- Far field stress σ_{yy}
- Accuracy of crack tip stress field with J-integral

$$J = \oint_s \frac{1}{2}\sigma_{ij}\varepsilon_{ij} - \sigma_{ij}\frac{\partial u_i}{\partial x} n_j ds$$

Accuracy of crack tip stress field

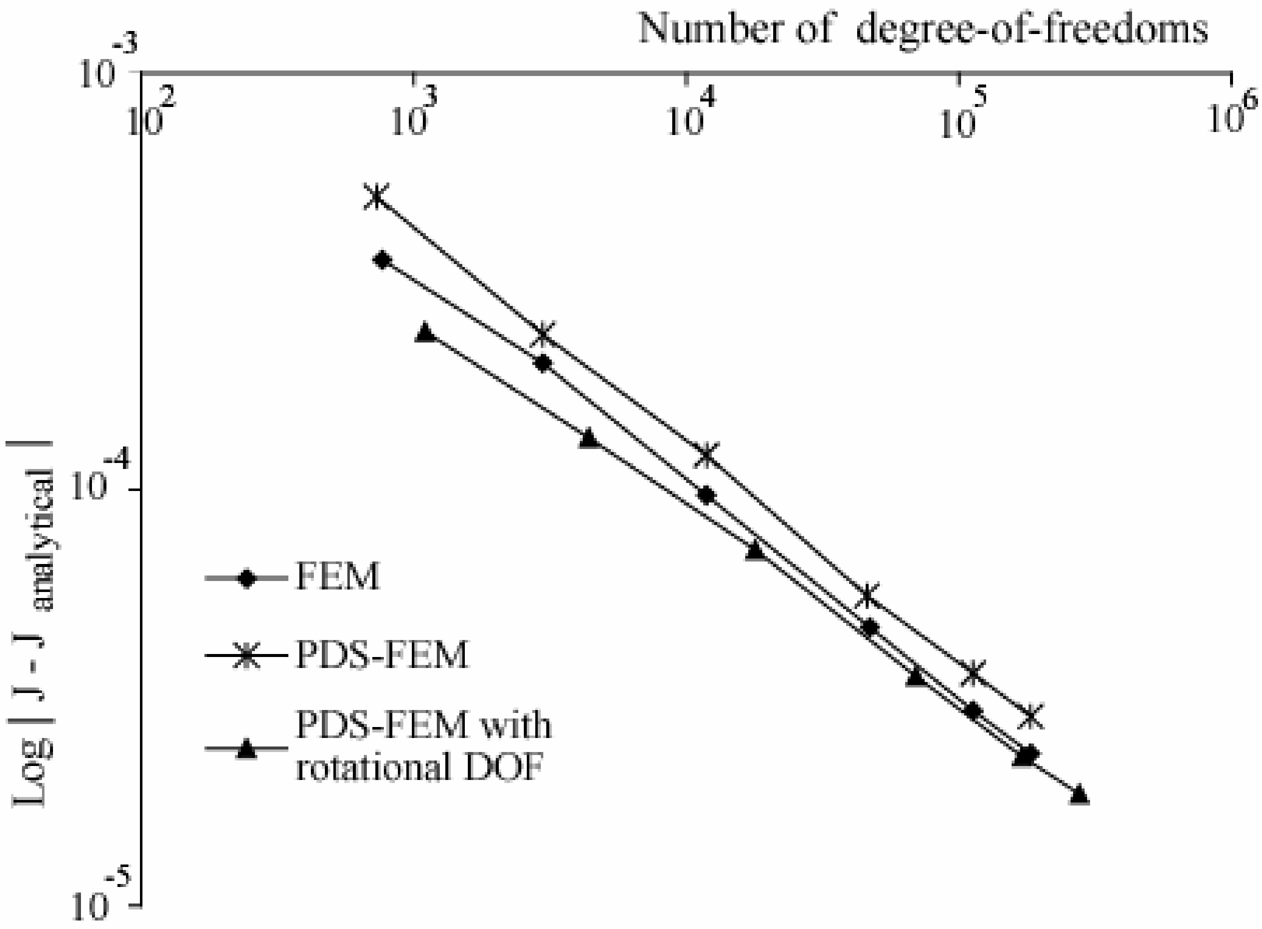

PDS-FEM crack tip stress filed is as accurate as the FEM solution, regardless of approximate failure treatment. The accuracy of crack tip stress filed can be improved by including rotational DOF

Accuracy of rotational component

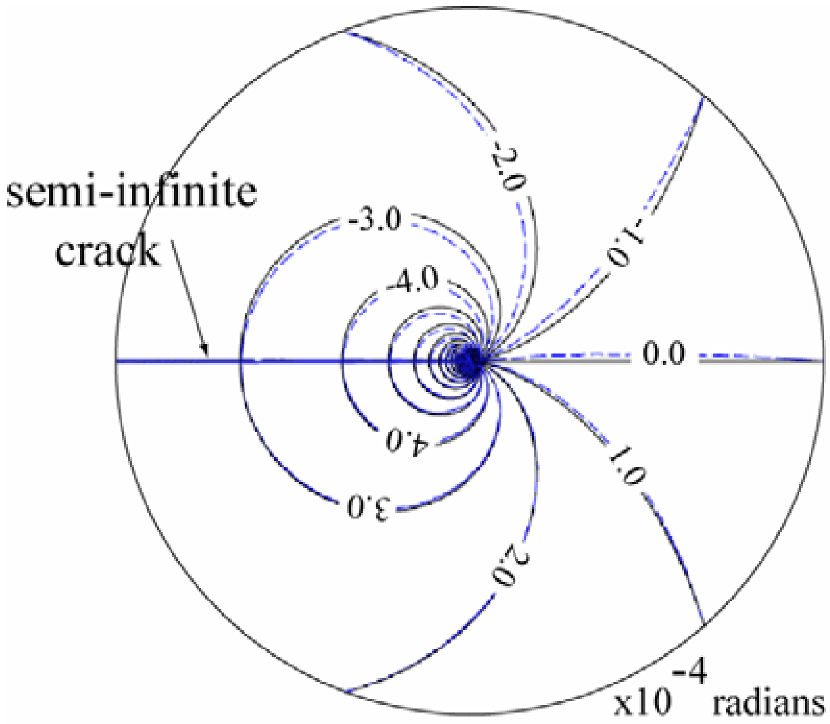

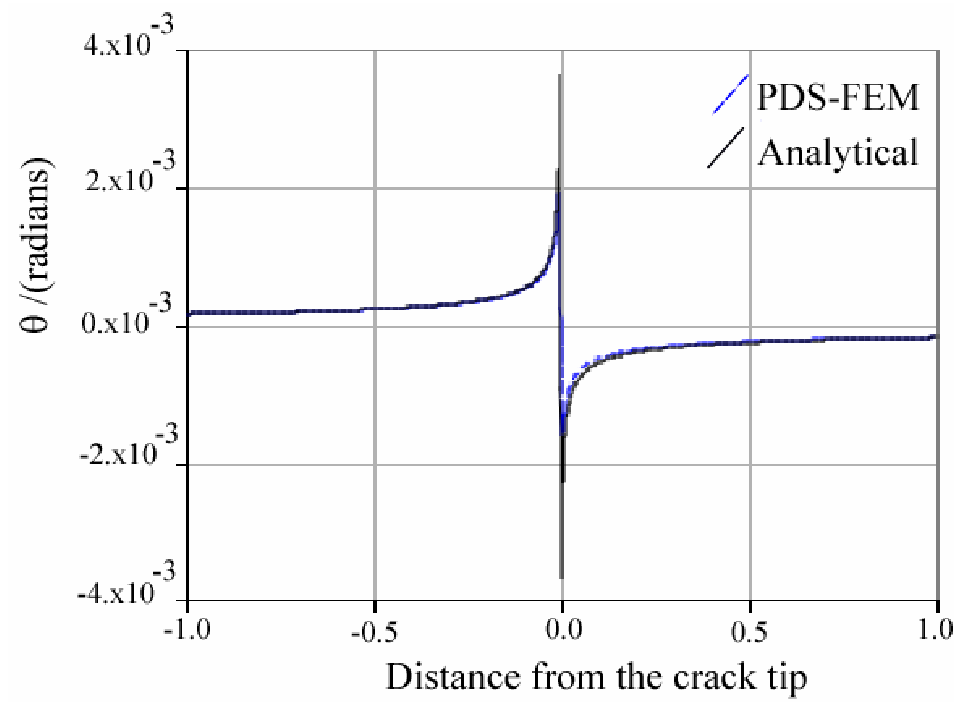

PDS-FEM estimates the rotational component fairly accurately, leading to better estimation of crack tip stress filed

Example problem: torsion testing

- Problem setting: torsion testing

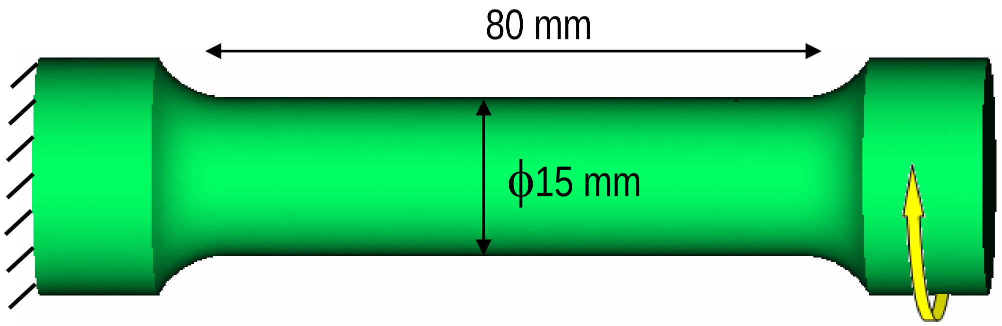

Real experiment

Helical spiral fracture surface

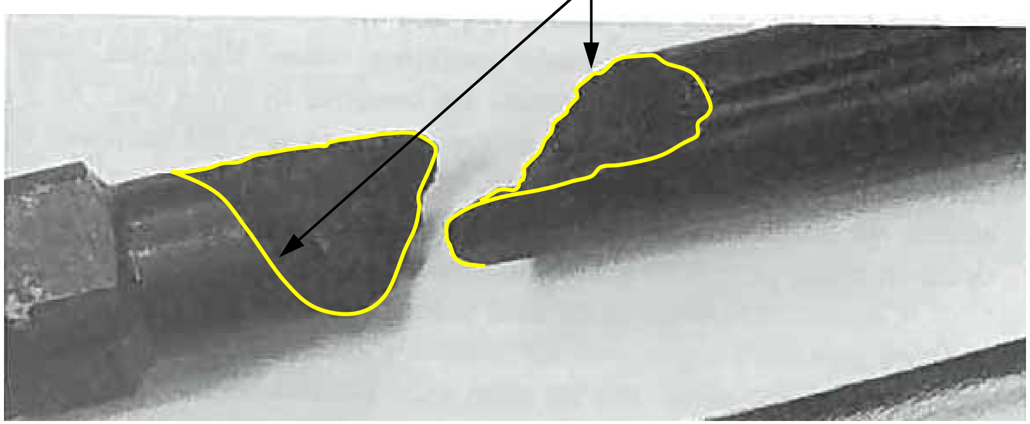

$E = 70\text{GPa}$

$\nu = 0.3$

Example problem: torsion testing

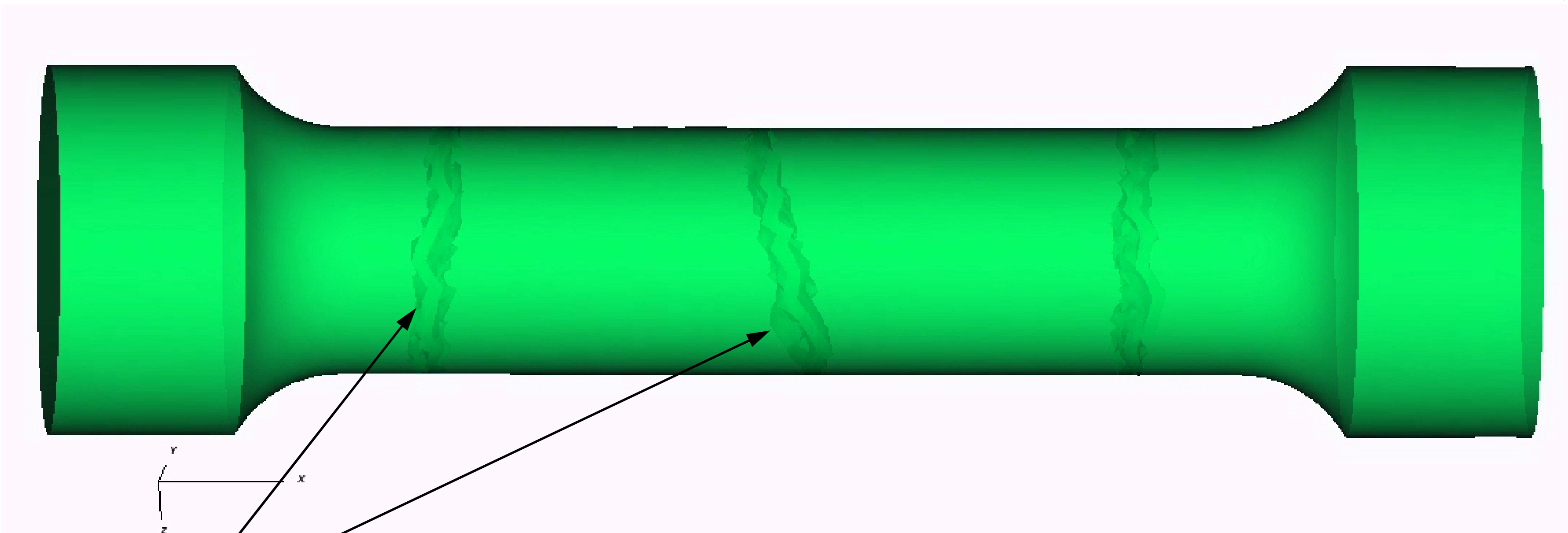

Ghost layer
(computed using MPI)

Helical spiral fracture surface

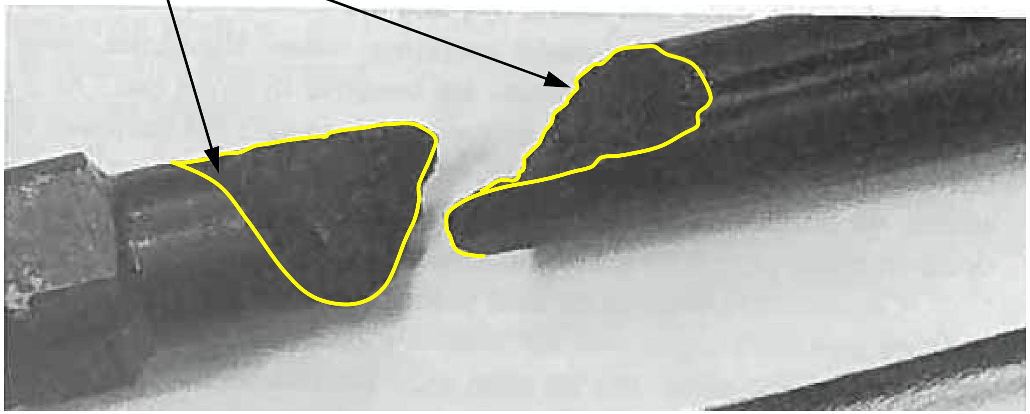

Organization

- Discretization scheme and formulation of PDS-FEM
- Failure treatment with torsional failure as an example
- Dynamic model and kidney stone breaking as an example

Time integration approaches for PDS-FEM

FEM like continuum representation

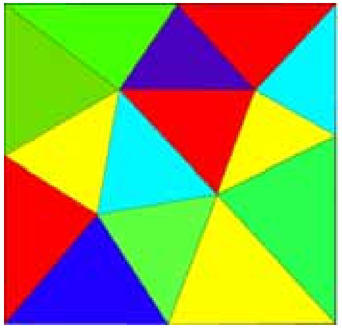

N-body problem like particle representation

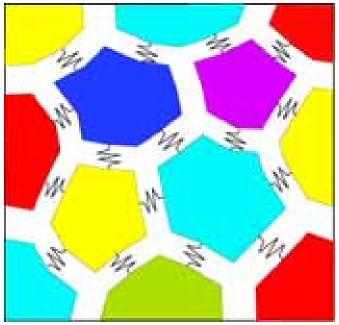

Lagrangian based

$$L = T - V = \sum_{\alpha} \frac{1}{2} m^{\alpha} \dot{u}_i^{\alpha} \dot{u}_i^{\alpha} - \sum_{\alpha} \frac{1}{2} K_{ij}^{\alpha'\alpha} u_j^{\alpha'} u_i^{\alpha}$$

Hamiltonian principle

$$\delta \int_{t_0}^{t_1} L(q, \dot{q})\, dt + \int_{t_0}^{t_1} F(q, \dot{q}).\delta q\, dt = 0$$

$$\downarrow$$

Second order explicit algorithm
(a range of Variational integrators)

Hamiltonian based

$$H = T + V = \sum_{\alpha} \frac{1}{2} m^{\alpha} \dot{u}_i^{\alpha} \dot{u}_i^{\alpha} + \sum_{\alpha} \frac{1}{2} K_{ij}^{\alpha'\alpha} u_j^{\alpha'} u_i^{\alpha}$$

Candy's method: 4th order symplectic

$$\mathbf{p}^k = \mathbf{p}^{k-1} + b^k \mathbf{F}(\mathbf{q}^{k-1}) \Delta t$$
$$\mathbf{q}^k = \mathbf{q}^{k-1} + a^k \mathbf{P}(\mathbf{p}^{k-1}) \Delta t \quad k = 1, .., 4$$

$$\mathbf{F}(\mathbf{q}) = -\frac{\partial V(\mathbf{q})}{\partial \mathbf{q}} \qquad \mathbf{P}(\mathbf{p}) = \frac{\partial T(\mathbf{p})}{\partial \mathbf{p}}$$

$$q_i^{\alpha} = u_i^{\alpha} \qquad p_i^{\alpha} = m^{\alpha} \dot{u}_i^{\alpha}$$

Simulating failure of concrete wall under tsunami load

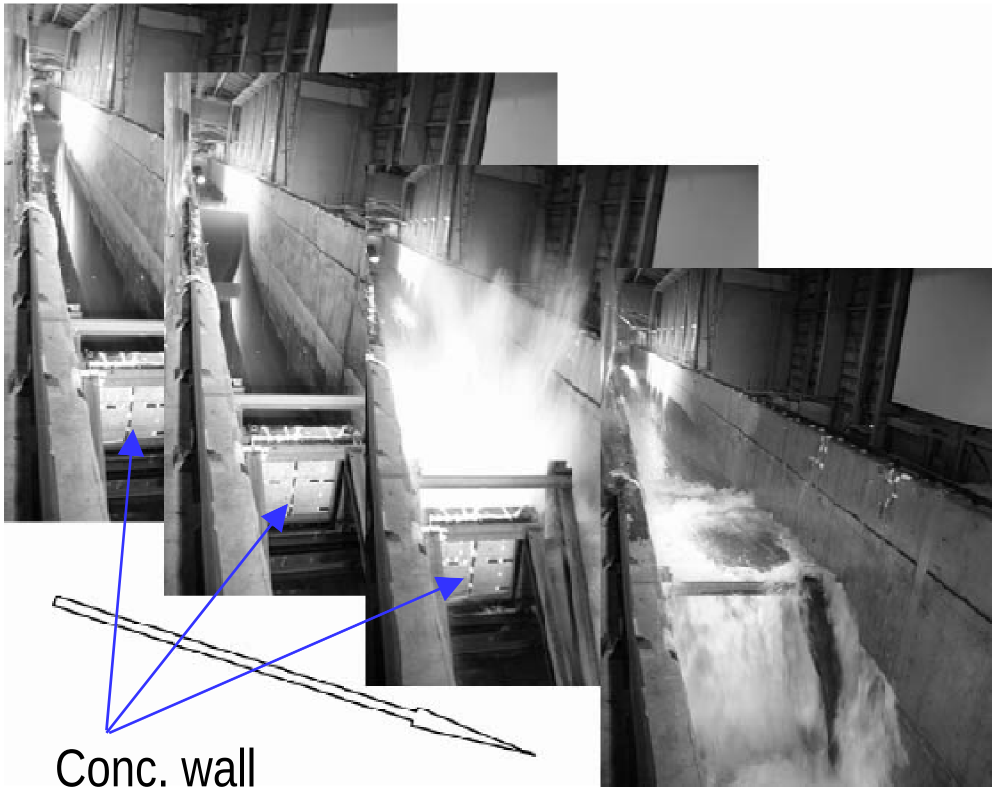

Snaps of the experiment

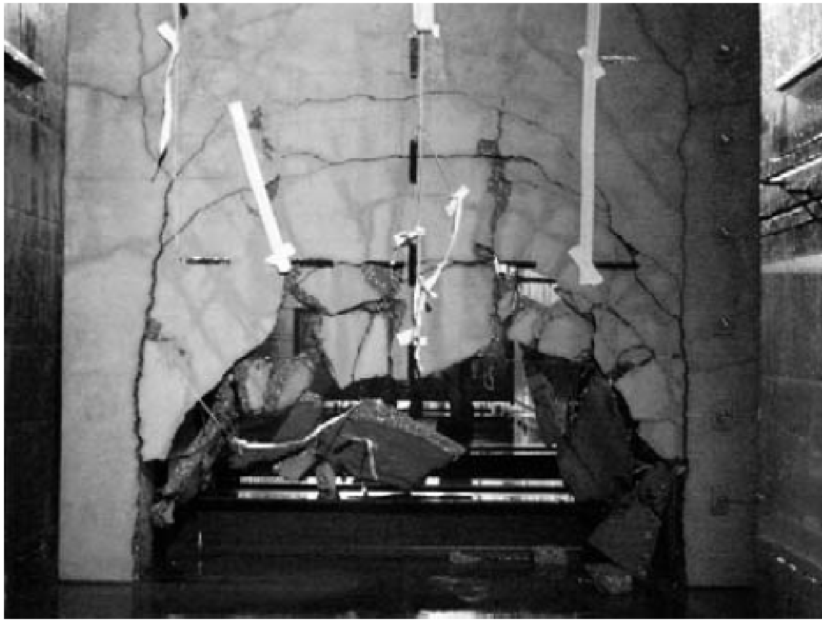

Damaged concrete wall

Conducted at the LHC facility at the Port and Airport Research Institute , Japan

Model details

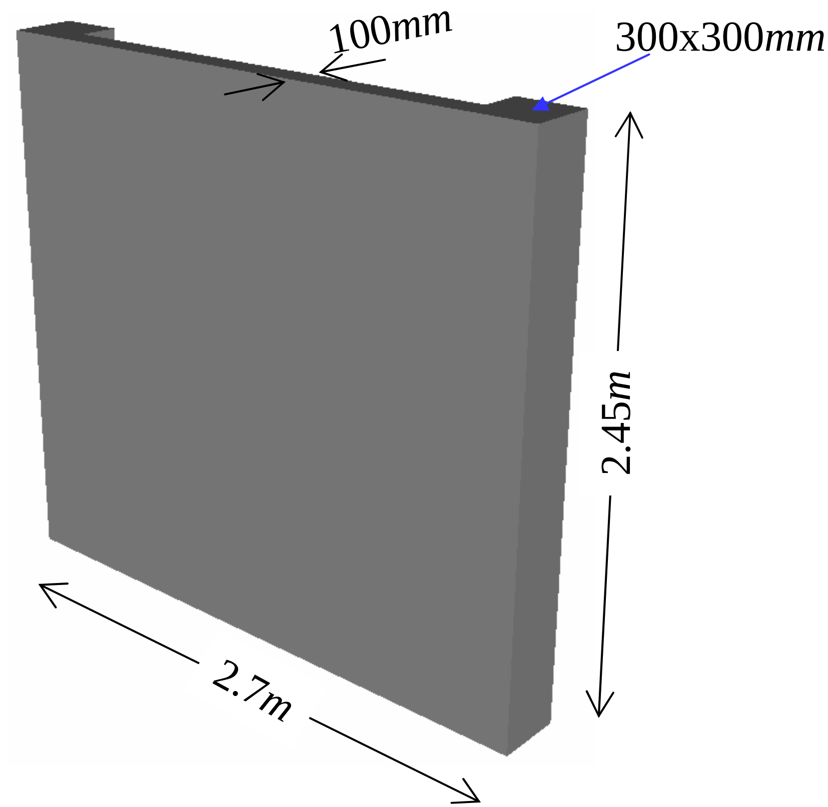

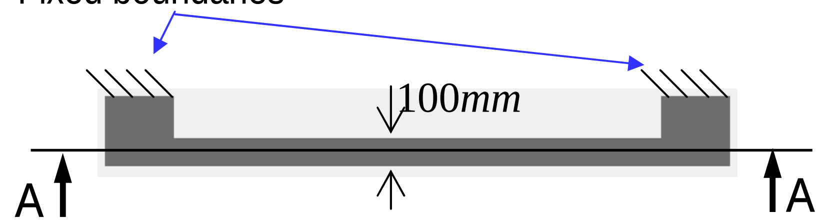

Section A-A

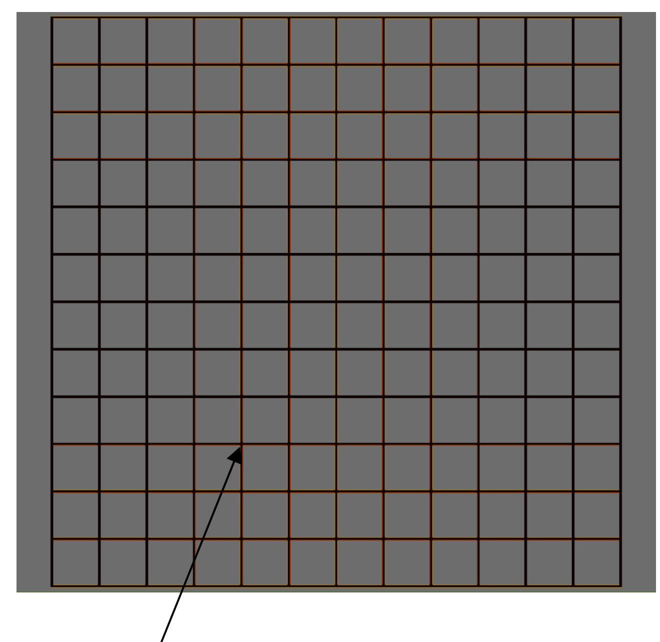

Reinforcement mesh (ϕ6@200mm x 200mm)

Material parameters

	Concrete	Steel
E /(GPa)	30	210
ν	0.2	0.3
σ_t /(MPa)	5	400

Input data: pressure time histories at 5 heights

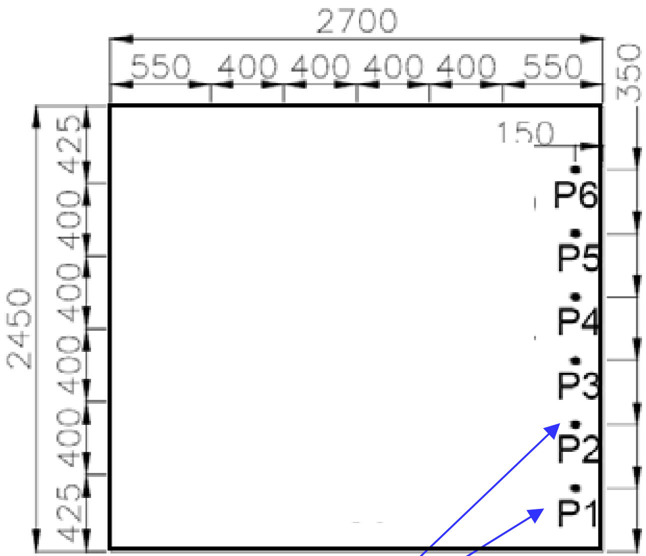

Locations of pressure gauges

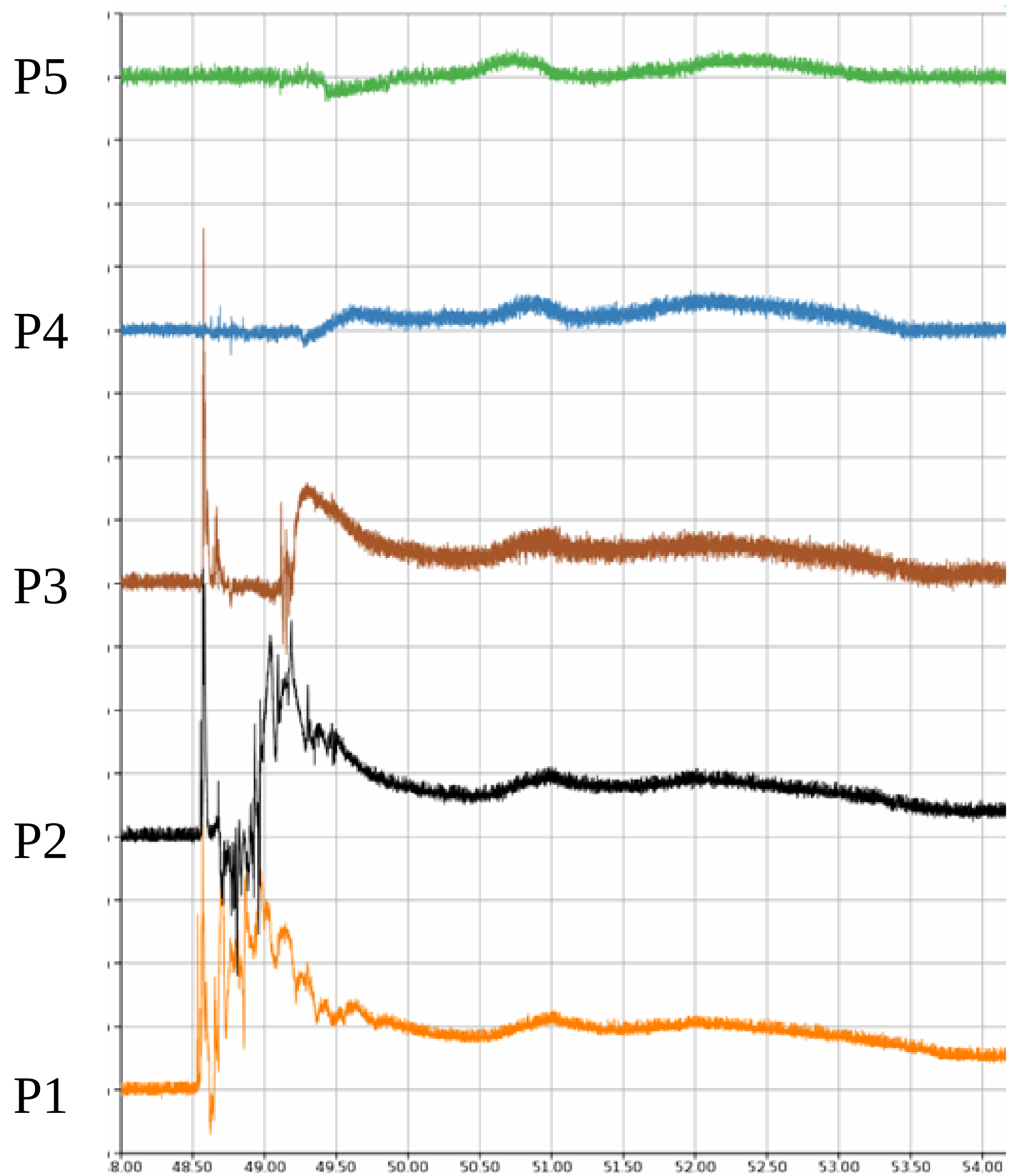

Pressure histories are interpolated for the intermediate points

Crack patterns : front side of 100mm thick wall

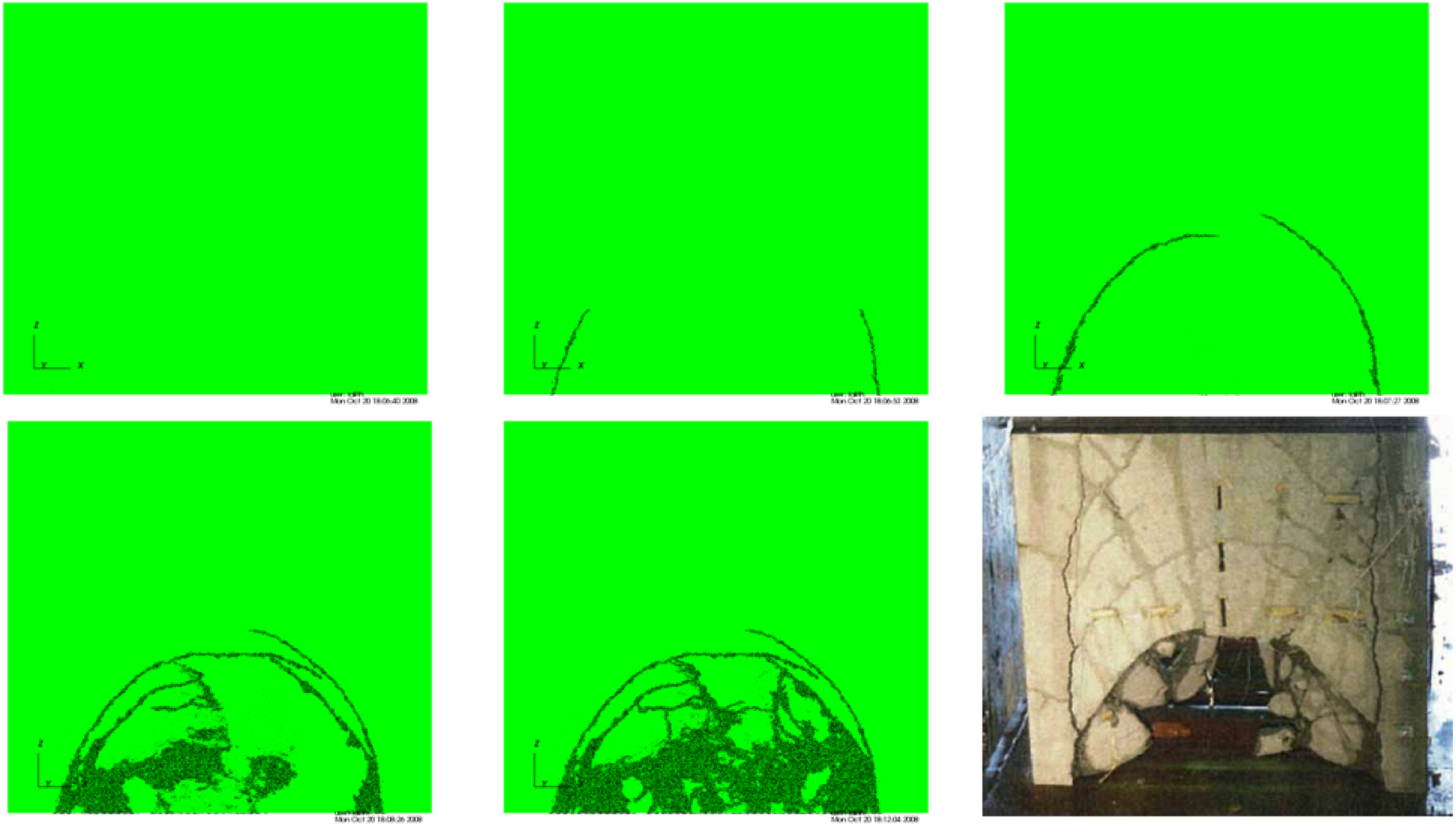

Crack patterns : back side of 100mm thick wall

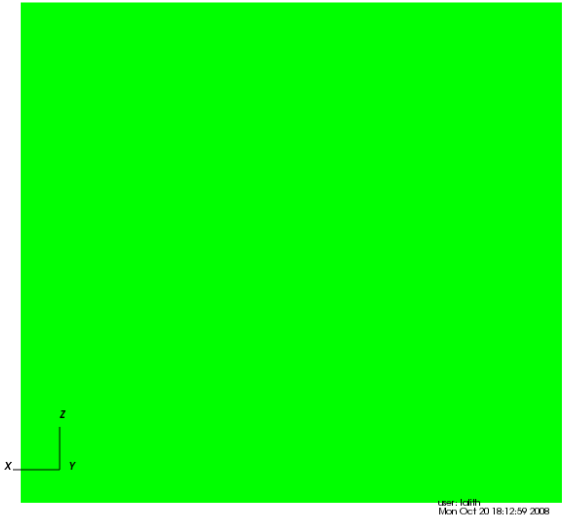

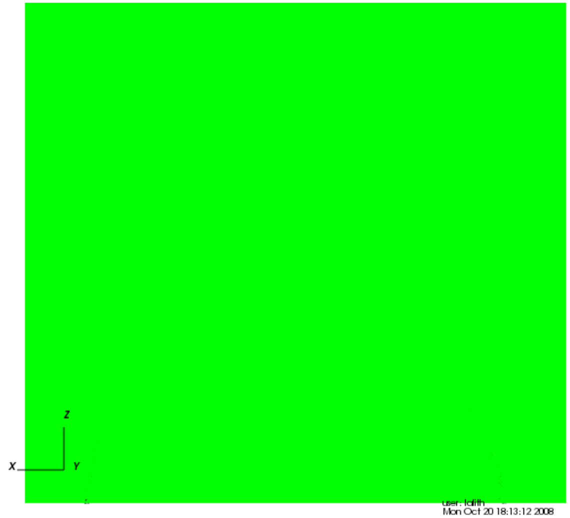

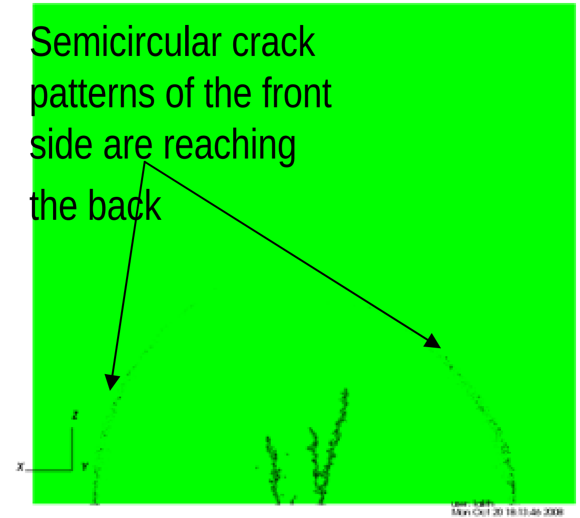

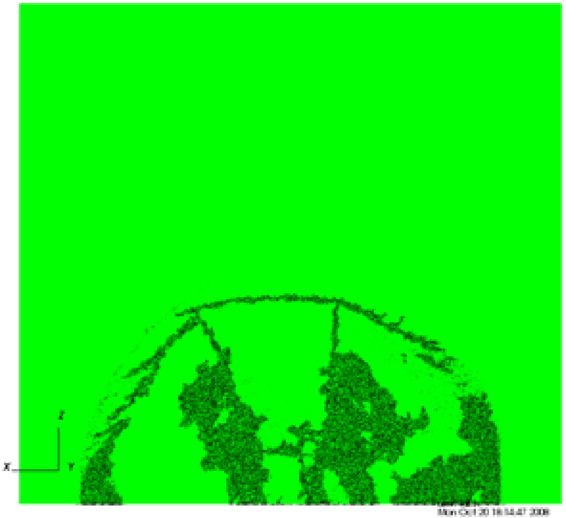

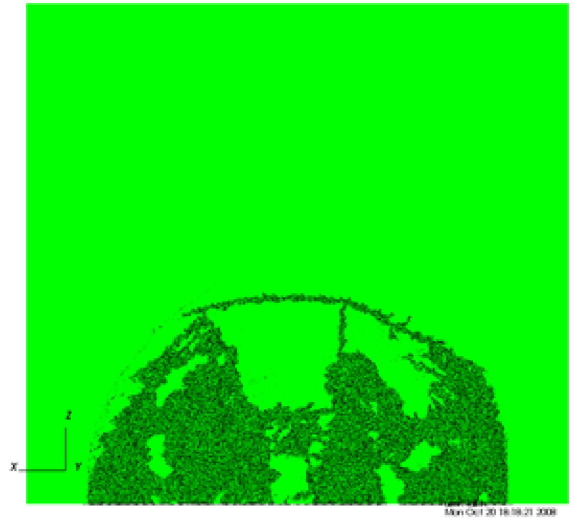

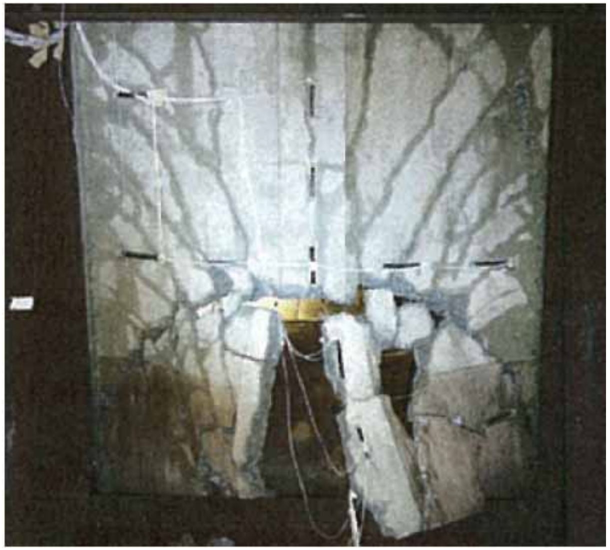

Shockwave Lithotripsy: kidney stone breaking

X-ray source

Ultrasonic pulse generator

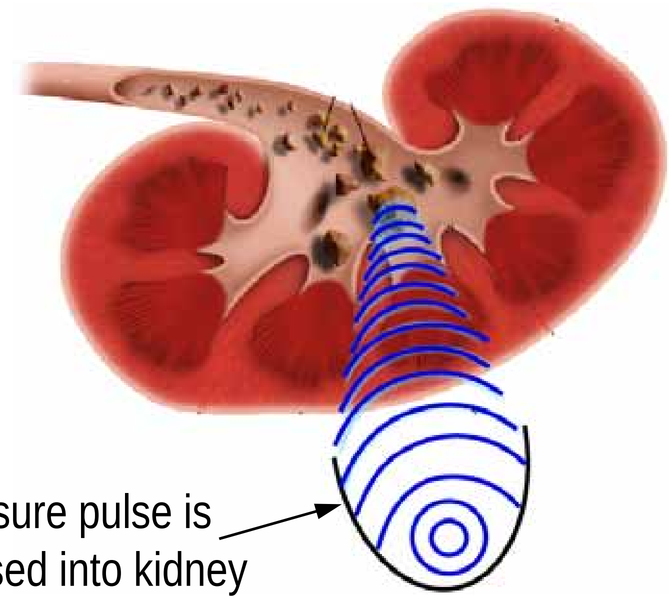

Pressure pulse is focused into kidney

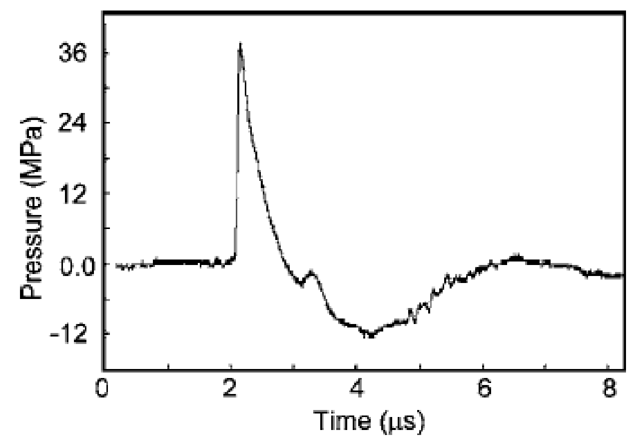

Typical pressure history in water induced by a single ultrasonic pulse

- Complete phenomena is not well explained
- Simulation of this mechanism would help further development of this technology

Current studies of Shockwave Lithotripsy (SWL)

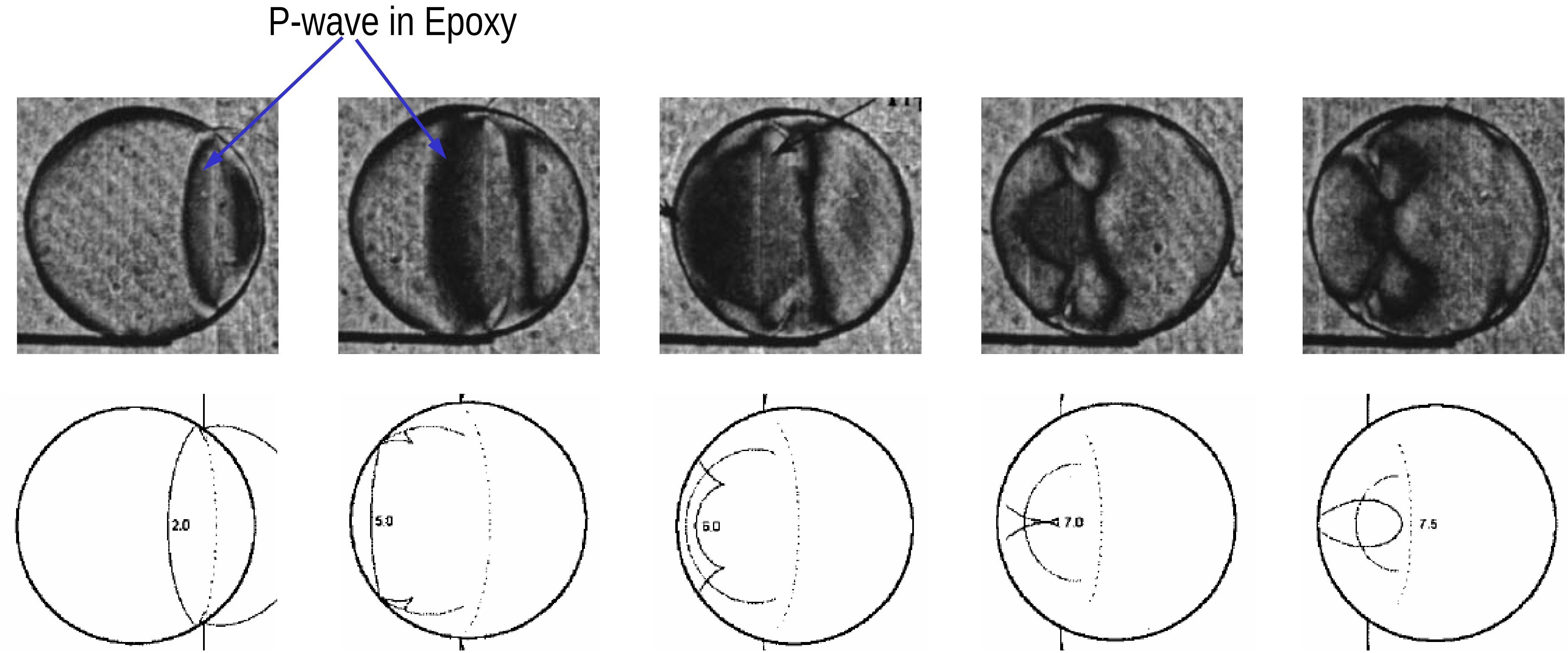

Xufeng Xi and Pei Zhong, J of Acoust. Soci. Am. 2001

- High speed photoelasticity and ray tracing are used to find the possible high stress regions and the locations of crack initiation
- Predicting the crack path of this dynamic phenomena has not yet been done

Interesting crack patterns in plaster of Paris samples

Cylindrical

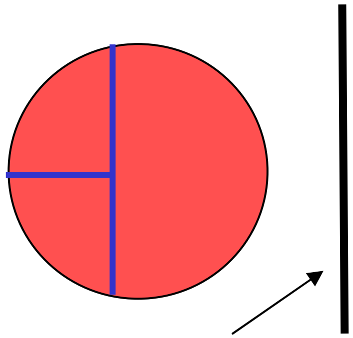

Plane wave

Rectangular prism

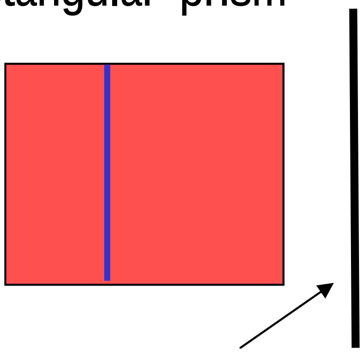

Plane wave

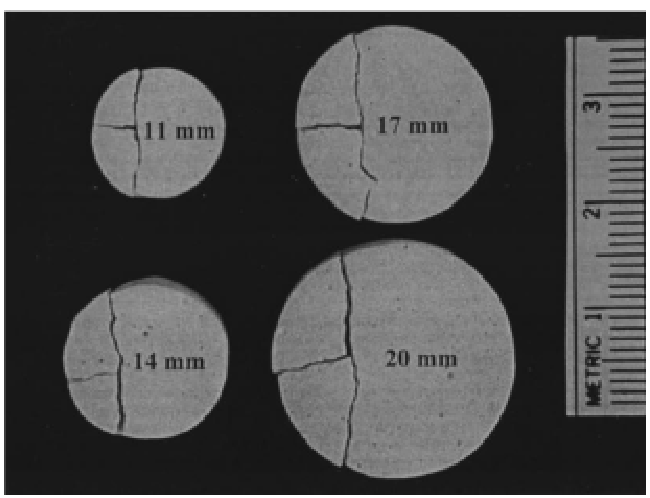

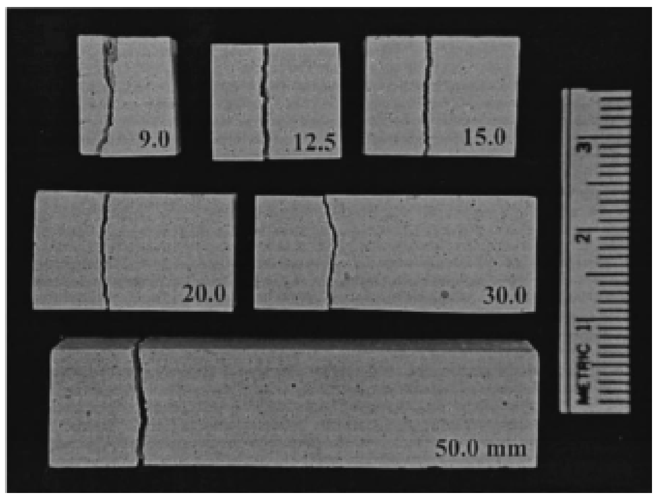

- Crack initiation and propagation is due to a dynamic state of stress
- This could be one of the toughest crack propagation problem to be simulated

Simulation of SWL: problem setting

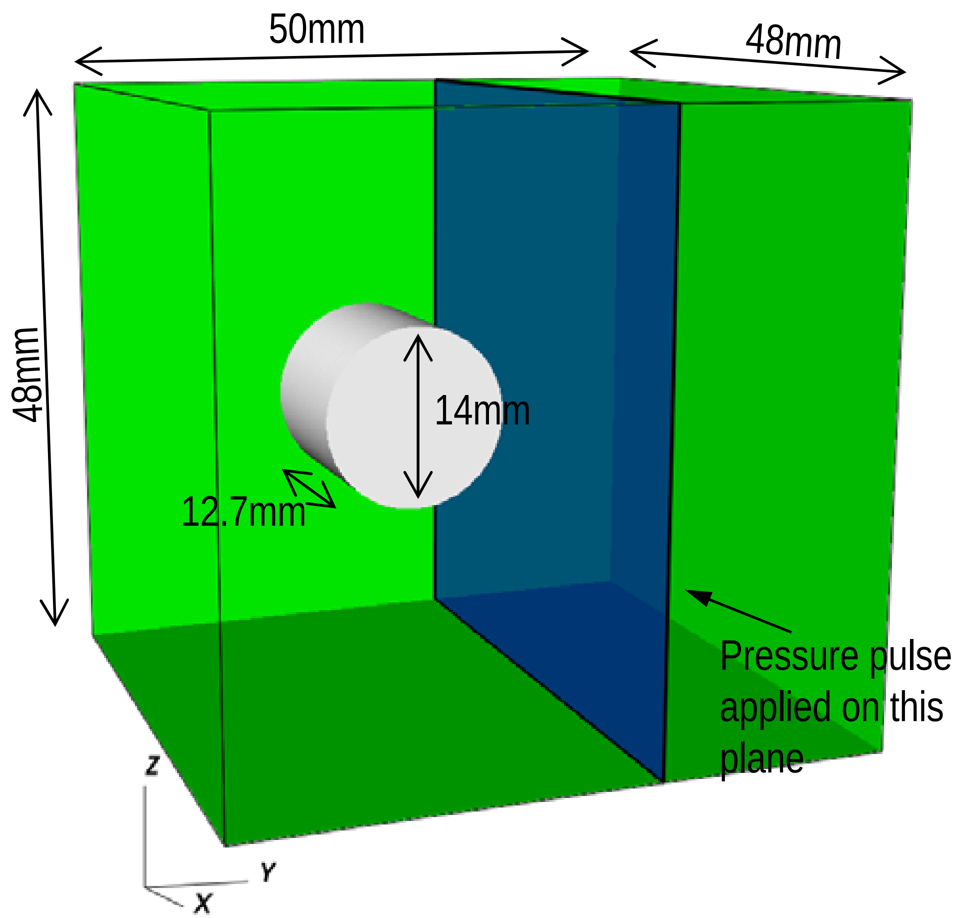

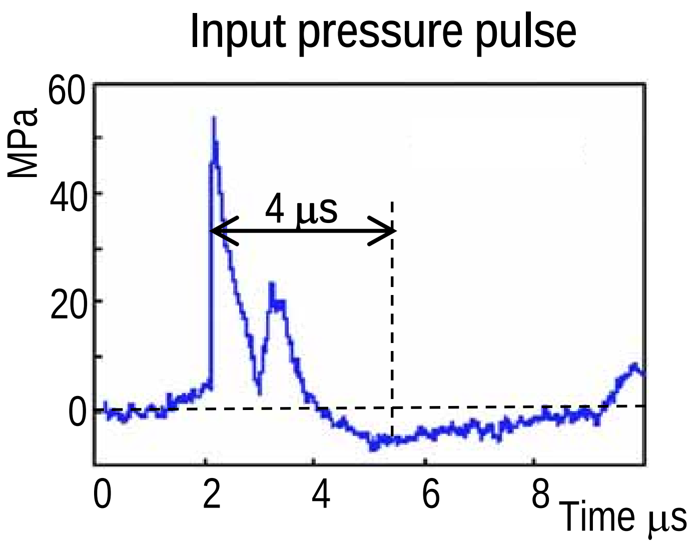

Yufeng Zhou and Pei Zhong, J. Acoust. Soc. Am.; 119(6) 2006

~ 6 million elements
~ 3.5 million DOFs

Plaster of Paris

E = 8.875 GPa
ν = 0.228
Vp = 2478 m/s
Vs = 1471 m/s

Water

K=
Vp = 1483 m/s

Stress waves of σ_{yy}

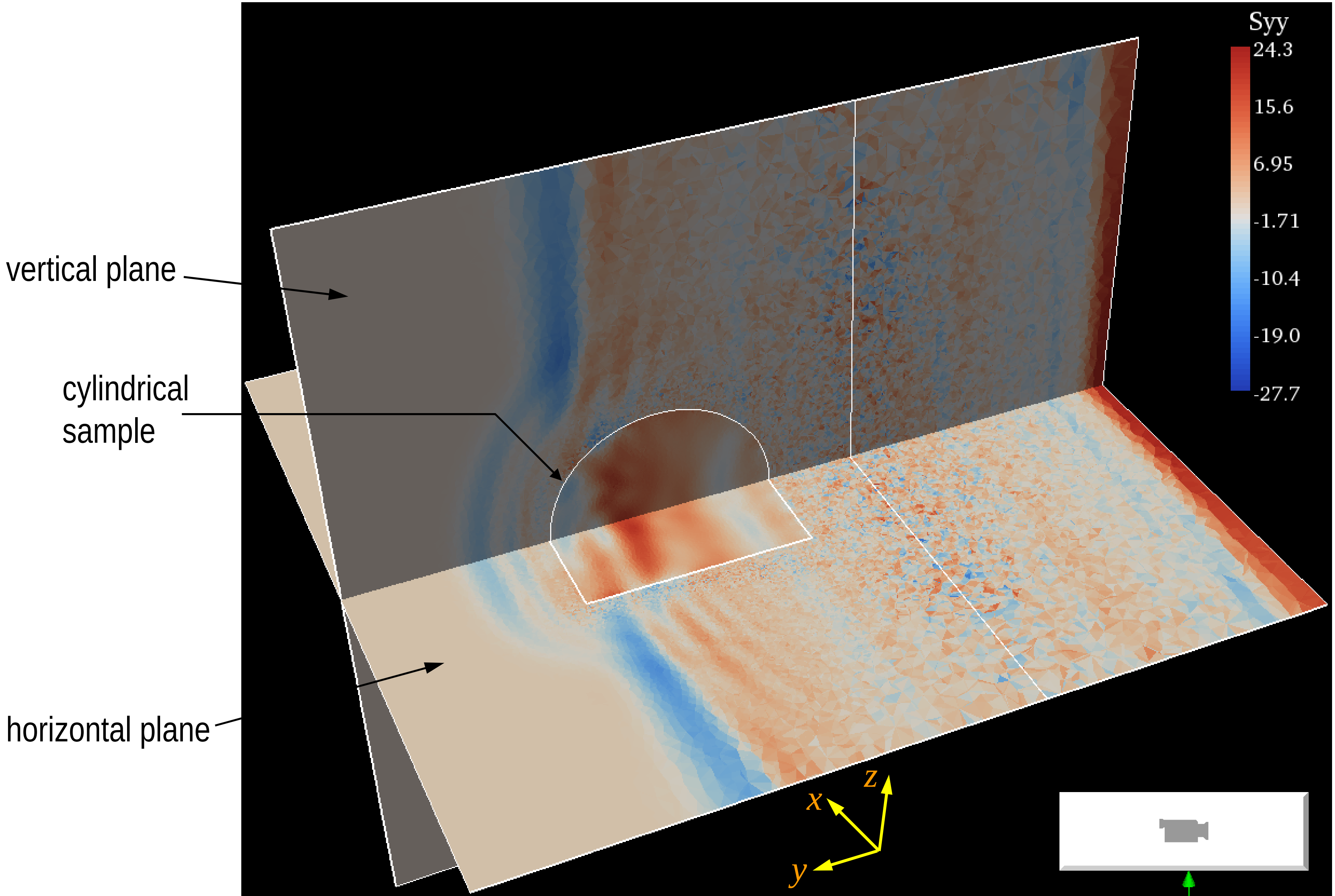

Crack patterns at different sections of cylinder

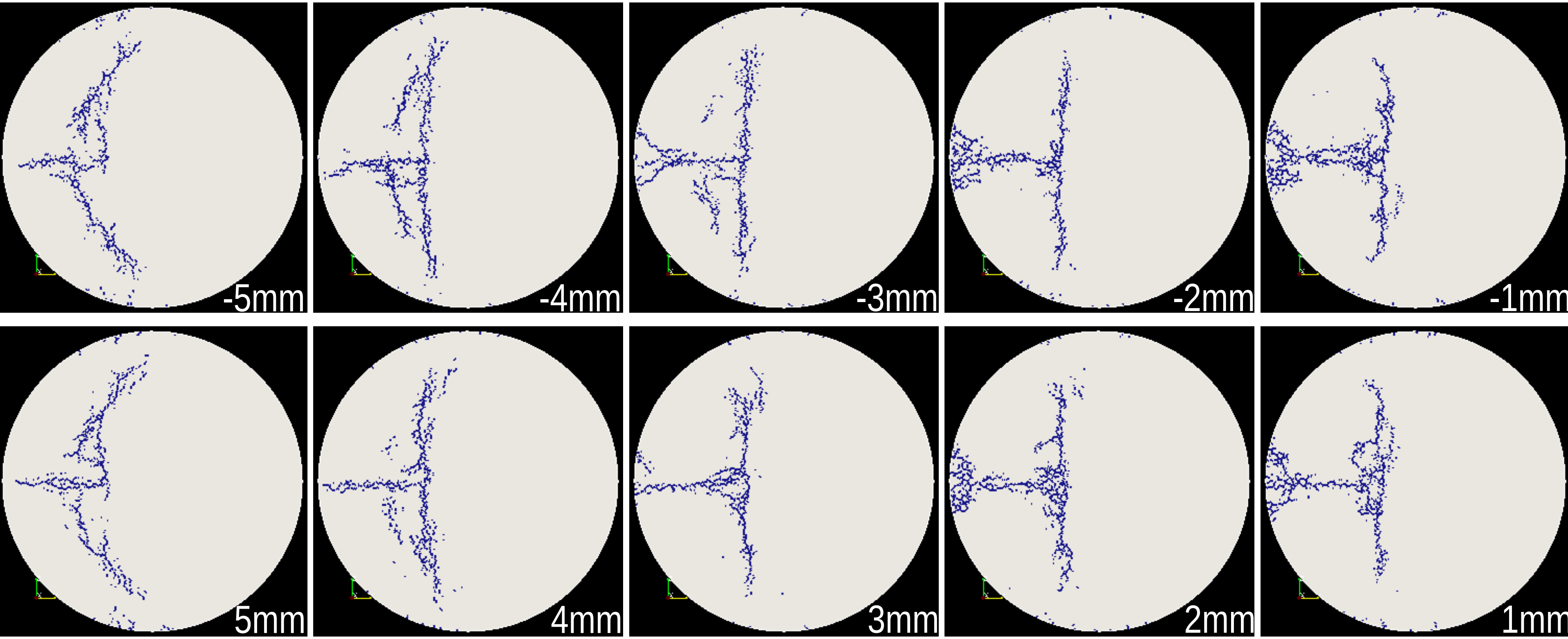

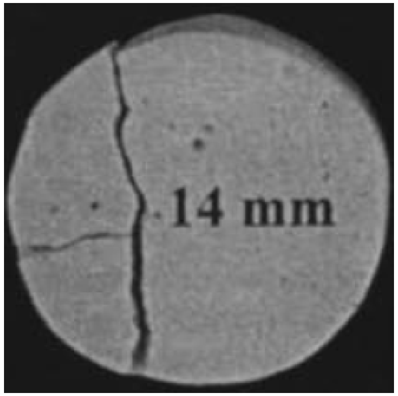

Tuler and Butcher failure criterion :

$$\int_0^t (\sigma_1 - \sigma_t)^2 dt \geq K_f$$

σ_t tensile strength

Summary

- Particle discretization for continuum mechanics problems
  - uses a set of non-overlapping characteristic functions on conjugate geometries
  - numerically efficient approximate failure treatment
  - accuracy of crack tip stress field can be improved with rotational DOF
  - particle physics type dynamic simulations (i.e. a simplified N body problem)

- We simulated several 3D crack profiles with complicated geometries